Title

Crustose coralline algae biomineral-bound nitrogen isotopes provide a baseline to reconstruct coral trophic strategies

Journal

Communications Earth & Environment, 7(1)

ISSN

2662-4435

Authors

Jung, Jonathan

Wald, Tanja

Foreman, Alan D

et al.

Publication Date

2026-04-10

DOI

10.1038/s43247-026-03459-2

communications earth & environment

Article

A Nature Portfolio journal

https://doi.org/10.1038/s43247-026-03459-2

Crustose coralline algae biomineral-bound nitrogen isotopes provide a baseline to reconstruct coral trophic strategies

Jonathan Jung[1] ✉, Tanja Wald[1], Alan D. Foreman[1], Aaron L. Bieler[1,2], Dorte Janussen[3], Simone Moretti[1,4], Nicolas N. Duprey[1,5], Dario Marconi[6], Carmen Pérez-Medina[7], Aaron O'Dea[7,8], Ralf Schiebel[1], Jochen Halfar[9], Cindy Fernández-García[10], Madeline Berger[11], Mary K. Donovan[11], Amy E. Frazier[12], Katie Cramer[7,13], Gerald H. Haug[1,2], Daniel M. Sigman[6] & Alfredo Martínez-García[1] ✉

Coral resilience is shaped by trophodynamic flexibility – the balance between photosymbiont-derived energy and feeding-based heterotrophy – yet quantifying this balance across taxa and through time remains difficult. Nitrogen (N) isotopes are a powerful tool to investigate trophic strategies, but their use requires information on local isotopic baselines. Here, we introduce the biomineral-bound N isotopes of crustose coralline algae (CCA) as an archive that closely tracks the N isotopic composition of the reef nitrate supply, making it a proxy for a reef's isotopic baseline. Coupled N isotope measurements of co-occurring CCA, symbiont-bearing, and symbiont-barren corals further enable us to quantify a coral's "trophic enrichment factor," reflecting the efficiency of the internal N recycling between the coral and its photosymbionts. From this framework, we derive a Reliance on Symbionts Index (RSI) that captures taxonomic and regional variation in mixotrophy, enabling reconstruction of coral trophodynamics in modern and fossil reef systems.

The marine nitrogen (N) cycle is a cornerstone of ocean biogeochemistry, playing a central role in the function of marine ecosystems and the ocean's biological carbon pump[1]. While most of the N in the ocean is biologically inert N_2, the inventory of biologically available (or 'fixed') nitrogen is supplied by N_2 fixation, the conversion of N_2 to organic N by N_2 fixing bacteria, and it is lost largely by denitrification, the reduction of the most oxidized form of N, nitrate, to N_2 as part of respiration in oxygen-poor environments. Fixed N undergoes a vigorous set of nested cycles within the ocean: Nitrate is supplied from the subsurface to the surface, where it is assimilated and recycled in surface waters, ultimately to be exported as organic N to the ocean interior, where remineralization and nitrification return it to nitrate. These processes control the spatiotemporal variations in the availability of fixed N in the ocean[2,3].

The stable isotopes of N (expressed as $\delta^{15}N = [(^{15}N/^{14}N)_{sample} / (^{15}N/^{14}N)_{air} - 1]*1000$ in ‰) can record changes in the global marine N cycle[4,5]. N_2 fixation introduces fixed N to the ocean with a $\delta^{15}N$ value of around −1‰[6], while the $\delta^{15}N$ of ocean nitrate is substantially higher (with a mean global pycnocline nitrate $\delta^{15}N$ of ~6.2‰[7]). This difference is largely due to water-column denitrification occurring in the ocean's oxygen-deficient zones, which preferentially removes ^{14}N from the nitrate pool, thereby raising the residual nitrate in $\delta^{15}N$[8,9]. In contrast, sedimentary denitrification typically fully consumes nitrate within the sediment pore

[1]ClimateGeochemistry Department, Max Planck Institute for Chemistry, Mainz, Germany. [2]Department of Earth and Planetary Sciences (D-EAPS) ETH Zürich, Zürich, Switzerland. [3]Senckenberg Research Institute and Natural History Museum Frankfurt, Frankfurt am Main, Germany. [4]Istituto di Scienze Polari, Consiglio Nazionale delle Ricerche, Bologna, Italy. [5]University of Brest, CNRS, IRD, Ifremer, LEMAR, Plouzané, France. [6]Department of Geosciences, Princeton University, Princeton, NJ, USA. [7]Smithsonian Tropical Research Institute, Balboa, Republic of Panama. [8]Secretaría Nacional de Ciencia, Tecnología e Innovación, Sistema Nacional de Investigación, Panama City, Panama. [9]Department of Chemical & Physical Sciences, University of Toronto at Mississauga, Mississauga, ON, Canada. [10]Centro de Investigación en Ciencias del Mar y Limnología, Escuela de Biología, Universidad de Costa Rica, San José, Costa Rica. [11]Hawai'i Institute of Marine Biology, University of Hawai'i at Mānoa, Kāne'ohe, Hawai'i, USA. [12]Department of Geography, University of California, Santa Barbara, CA, USA. [13]Center for Biodiversity Outcomes, Arizona State University, Tempe, AZ, USA. ✉e-mail: jonathan.jung@mpic.de; a.martinez-garcia@mpic.de

waters, preventing ^{15}N-enriched residual nitrate from escaping into the overlying water column[10]. Thus, despite exceptions under special circumstances[11], most sedimentary denitrification exerts a negligible influence on the $\delta^{15}N$ of overlying water-column nitrate[12].

The N isotopic composition of biomineral-bound organic matter (BB-$\delta^{15}N$) in foraminifers[13–16], diatoms[17,18], and corals[19,20], predominantly reflects the isotopic composition of the nitrate supplied and consumed in the surface ocean. In addition, biomineral-bound organic matter is protected from diagenesis by the biomineral matrix[21]. Thus, the BB-$\delta^{15}N$ proxies can be used to reconstruct past changes in the N cycle across a wide range of timescales, from decades to millions of years[22–27]. Beyond reflecting external N sources, however, BB-$\delta^{15}N$ also encodes key physiological differences among organisms. Typical heterotrophs, including symbiont-barren foraminifera and corals, preferentially metabolize ^{15}N-depleted organic matter and excrete the resulting low-$\delta^{15}N$ ammonium, elevating the $\delta^{15}N$ of the remaining tissue (and, thus biomineral-bound N) by 2 to 5‰ relative to their diet[24,28–31]. In contrast, symbiont-bearing foraminifera and corals maintain tight metabolic coupling with photosynthetic dinoflagellates (family *Symbiodiniaceae*), which reassimilate the host-produced metabolic ammonium and thus prevent its excretion to the environment, resulting in BB-$\delta^{15}N$ values that closely track ambient N source values[13,19,24,28].

These trophic isotopic effects have been instrumental in diagnosing the presence or absence of photosymbiosis in modern and fossil coral communities[24,31,32]. However, such comparisons lack independent, autotrophic reference points to anchor interpretations of coral trophic behaviour. Mixotrophic species, which combine autotrophy and heterotrophy, may exhibit a fraction of the full trophic enrichment typical of obligate heterotrophs (i.e., +2 to 5‰)[33–35]. In a catabolic-anabolic framing, this occurs because a portion of ingested N is shed catabolically via ^{14}N-rich excretion, while another portion is retained anabolically, yielding intermediate $\delta^{15}N$ values[36]. This mixotrophic strategy – feeding partially uncoupled from the nutrient demands of the endosymbionts and thus leading to nutrient excretion – can enhance coral resilience under stress by compensating for declines in symbiont-derived energy (Fig. 1)[33].

Despite its ecological significance, quantifying the reliance on photosymbionts across coral taxa remains methodologically challenging. Current approaches include gut content analysis[37], laboratory feeding experiments[38], molecular techniques[39], and stable isotope studies to estimate the proportional contribution of autotrophic (symbiont-derived, mostly metabolically recycled) versus heterotrophic (directly prey-derived) N to the coral host[40,41]. While these methods have provided valuable insights, they also face limitations. Many are labour-intensive, context-dependent, or fail to capture natural variability in feeding rates and preferences.

Moreover, nearly all current methods are constrained to modern reef systems and living corals, which limit our ability to assess reliance on

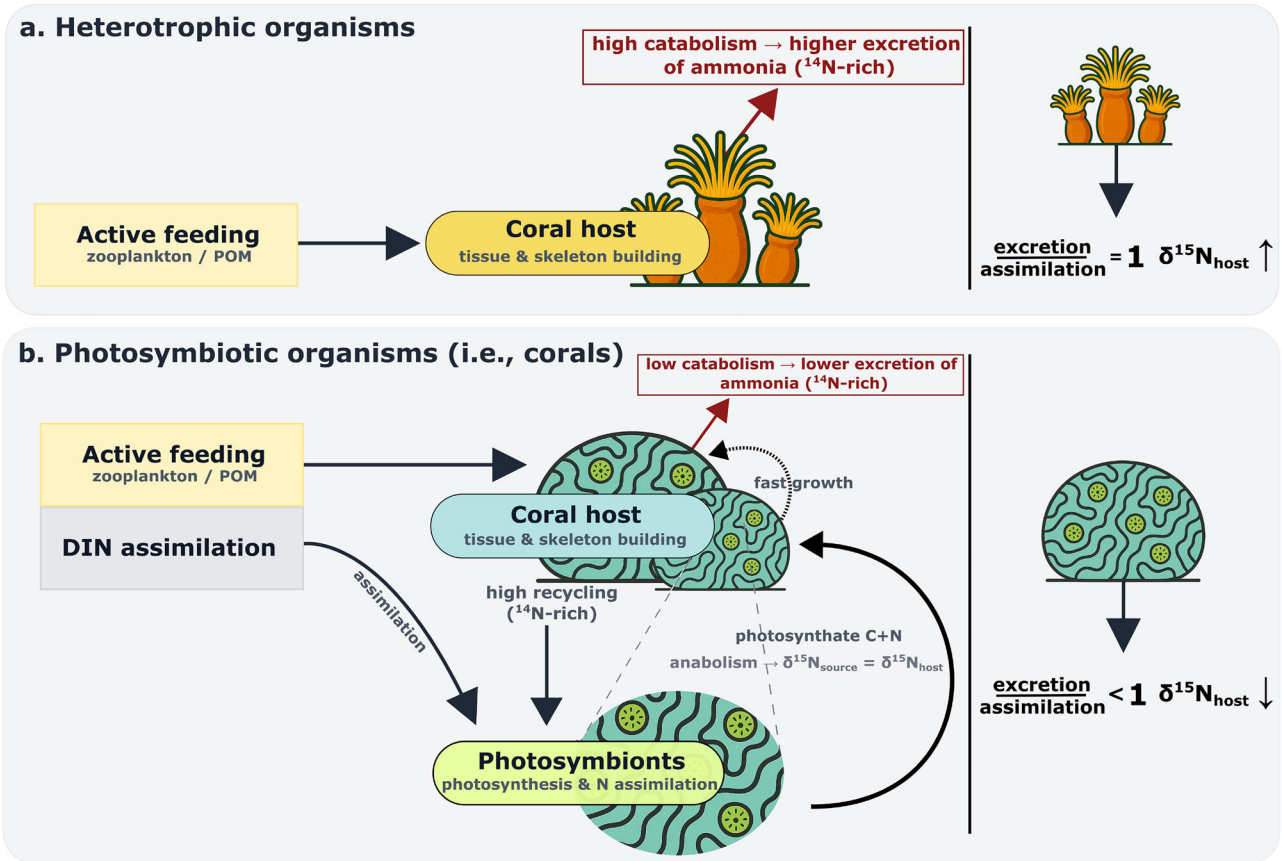

Fig. 1 | Nitrogen routing, metabolic state, and $\delta^{15}N$ in heterotrophic vs. photosymbiotic animals. a Prey or particulate organic matter (POM) is ingested by the coral host. During catabolism, deamination and excretion preferentially remove ^{14}N as ammonium, enriching retained body N in ^{15}N and elevating $\delta^{15}N_{host}$. In heterotrophic corals, as in heterotrophs in general, these are the dominant dynamics in setting their $\delta^{15}N$ relative to their feeding sources. **b** In photosymbiotic corals, N sources include both feeding and the possibility of assimilating dissolved inorganic N (DIN, dominantly nitrate and ammonium). The photosymbionts acquire metabolic N waste from the host or the DIN assimilated from the environment, using it in their photosynthetic growth. Photosynthate C and N is transferred to the host, and a tight internal N recycling loop returns the ^{14}N-rich waste to the photosymbionts. Under anabolism (growth, stable photosymbiosis), recycling suppresses net ^{14}N loss, keeping $\delta^{15}N_{host}$ closer to the baseline N source (right-hand down arrow). Increased catabolism weakens N retention, increasing ^{14}N-rich excretion, raising $\delta^{15}N_{host}$. Arrows show assimilation, ingestion, symbiont-to-host transfer, excretion, and recycling; Overall, the $\delta^{15}N$ of corals relative to their environmental N sources reflects the balance between coral growth (anabolism) and excretion (catabolism), with photosymbiosis biasing the system toward N recycling, N retention for growth, and lowering $\delta^{15}N$.

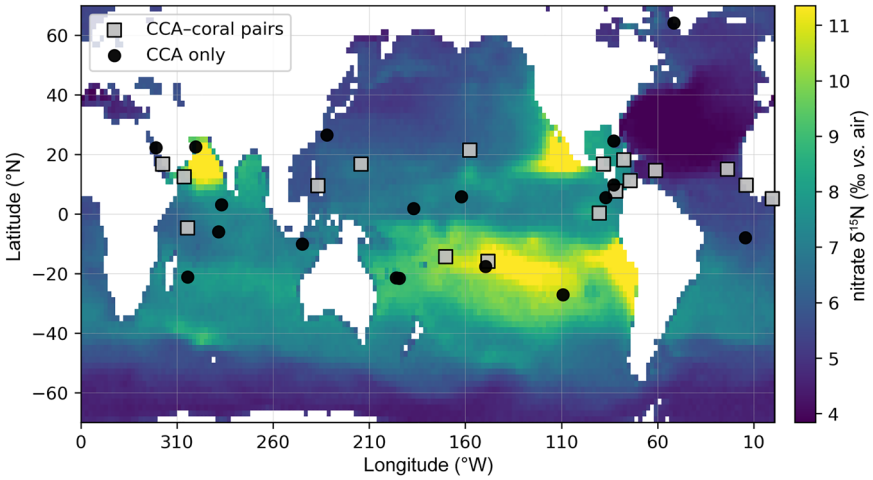

Fig. 2 | Locations of coralline algae-coral pairs with respect to average subsurface (200 m water depth) nitrate $\delta^{15}N$. Background shading shows nitrate $\delta^{15}N$ predicted by a neural network trained on the nitrate isotope compilation of Fripiat et al. (2021)[7]. The predicted field is presented only as a visual reference and was not used in calculations or statistical analyses. Sampling locations of coralline algae-coral pairs are indicated as grey squares. Locations where only coralline algae were obtained are indicated as black circles.

photosymbionts over historical timescales. As a result, the role of mixotrophic variation in coral persistence during past and ongoing environmental change remains largely speculative. There is a striking absence of proxies that allow reliance on photosymbionts to be inferred from the historical record[42]. This has left a major gap in our understanding of how mixotrophy evolved, how it has been selected for or against over time, and how it may have contributed to the long-term success or decline of different coral lineages[43,44]. Developing proxies for reconstructing trophic ecology beyond modern observations is therefore critical for contextualizing coral resilience in a historical framework.

In this context, crustose coralline algae (CCA) offer a promising new avenue. CCAs are a diverse group of red algae that play significant roles in marine ecosystems, both as free-living organisms and encrusting forms[45,46]. CCAs are characterized by their predominantly high-magnesium calcite precipitate[47], their slow growth rates, and their ability to reproduce both sexually and asexually, contributing to their resilience and adaptability[46]. Free-living CCA provide essential habitat and nursery grounds for various marine species, enhancing biodiversity, while encrusting CCA are crucial in consolidating and stabilizing reef structures, promoting coral settlement, and contributing to carbonate production[48]. As obligate photoautotrophs, CCA have the potential to record the $\delta^{15}N$ of their inorganic N sources without the metabolic alterations seen in mixotrophic or heterotrophic organisms[49]. Therefore, the CCA BB-$\delta^{15}N$ (hereafter $\delta^{15}N_{CCA}$) is a potentially powerful trophic baseline against which it becomes possible to constrain the degree of autotrophy versus heterotrophy within mixotrophic coral species.

The bulk tissue (i.e., not biomineral-bound) isotopic composition of some CCA species ($\delta^{15}N_{Bulk\text{-}CCA}$) has already been proposed as a proxy to reconstruct changes in the marine N cycle[50,51]. However, most of the organic material measured in this bulk CCA approach is not protected from diagenesis by the mineral matrix, and thus can be diagenetically altered, especially in deep geological settings[24]. In contrast, $\delta^{15}N_{CCA}$ is protected by the biomineral matrix, suggesting great potential for palaeoceanographic and Earth history reconstructions[21]. Accordingly, modern field and lab studies are needed to investigate the signals recorded in $\delta^{15}N_{CCA}$.

Here, we generate and compile N isotopic measurements of CCA and compare the data to the N isotopic composition of subsurface nitrate closest to their respective sampling locations (Figs. 2 and 3). We then use a subset of only encrusting CCA and compare them to the $\delta^{15}N$ values of co-occurring pairs of symbiont-bearing and symbiont-barren corals from the same location (Fig. 4). Through this approach, we demonstrate that these 'triplets' can be used to track past changes in the marine N cycle while simultaneously helping to infer reefal symbioses and degrees of heterotrophy across tropical ocean regimes.

Results

N isotope results

Across 30 tropical reef sites spanning the Indo-Pacific, Atlantic, Red Sea, and Caribbean, $\delta^{15}N_{CCA}$ values range from 2.65‰ to 10.29‰ (Figs. 2 and 3). In areas of complete nutrient consumption, $\delta^{15}N_{CCA}$ values show a positive correlation with the mean $\delta^{15}N$ of subsurface nitrate ($R^2 = 0.85$, $p < 0.001$) (Fig. 2).

The lowest $\delta^{15}N$ values are observed in oligotrophic regions where the low $\delta^{15}N$ of N_2 fixation causes the $\delta^{15}N$ of shallow subsurface (thermocline) nitrate to be lower than the mean pycnocline nitrate value (~6.2‰, Fripiat et al., 2021). These low values typically range between ~2.8‰ and ~5.5‰ and characterize sites such as Belize, New Caledonia, Jamaica, and the wider Caribbean and some Pacific Island regions. Higher $\delta^{15}N_{CCA}$ values are observed in areas with more rapid nitrate supply, especially upwelling, including the Seychelles, Cape Verde, Guinea, and the Galápagos, with values between ~6.3‰ and ~7.8‰. Even higher $\delta^{15}N_{CCA}$ values (>8‰) are recorded in regions such as southern Indonesia, Ghana, Japan, Socotra, Oman, and the Pacific coast of Panama. Notably, locations downstream of oxygen-deficient zones (ODZs) in the equatorial Pacific, such as Kiribati, Makatea, Palmyra, and American Samoa also show elevated $\delta^{15}N_{CCA}$ signatures. The British Indian Ocean Territory exhibits higher values than nearby Maldives sites, while Ascension Island mirrors the $\delta^{15}N$ of South Atlantic subsurface nitrate, consistent with broader oceanographic patterns (Fig. 2).

The 17 locations that allowed for triplet sample analysis from the same location (BB-$\delta^{15}N$ of CCA, symbiont-bearing and symbiont-barren corals) yield similar results for CCA and symbiont-bearing corals ($\delta^{15}N_{sym\text{-}coral}$). In contrast, symbiont-barren corals ($\delta^{15}N_{nonsym\text{-}coral}$) are always 2 to 5‰ enriched, consistent with the trophic enrichment factor[24,30] (Fig. 4).

The difference between $\delta^{15}N_{nonsym\text{-}coral}$ and $\delta^{15}N_{sym\text{-}coral}$ (expressed as $\Delta\delta^{15}N_{nonsym\ -\ sym}$), and the difference between $\delta^{15}N_{nonsym\text{-}coral}$ and CCA (expressed as $\Delta\delta^{15}N_{nonsym\ -\ CCA}$) allows us to investigate whether the trophic enrichment factor is consistent across sites or whether the feeding behavior of symbiont-bearing corals changes due to varying feeding sources, thus, affecting the level of mixotrophy (Supplementary Fig. 2). $\Delta\delta^{15}N$ values vary between 1.72‰ to 5.1‰ for $\Delta\delta^{15}N_{non\text{-}sym\ -\ sym}$ and between 2.49‰ to 5.49‰ for $\Delta\delta^{15}N_{non\text{-}sym\ -\ CCA}$ across the 17 locations (Fig. 4a). However, comparing the average values of $\Delta\delta^{15}N_{non\text{-}sym\ -\ sym}$ (3.26‰ ±1.07) and $\Delta\delta^{15}N_{non\text{-}sym\ -\ CCA}$ (3.68‰ ±0.97) taken from all triplet locations yields no significant difference in variability or averages ($t = 0.065$, $p = 0.79$) (Fig. 4b).

Discussion

CCA as a proxy to reconstruct the marine N cycle

CCA are increasingly recognized for their capacity to provide insights into long-term ecological and climatic shifts through their central role as

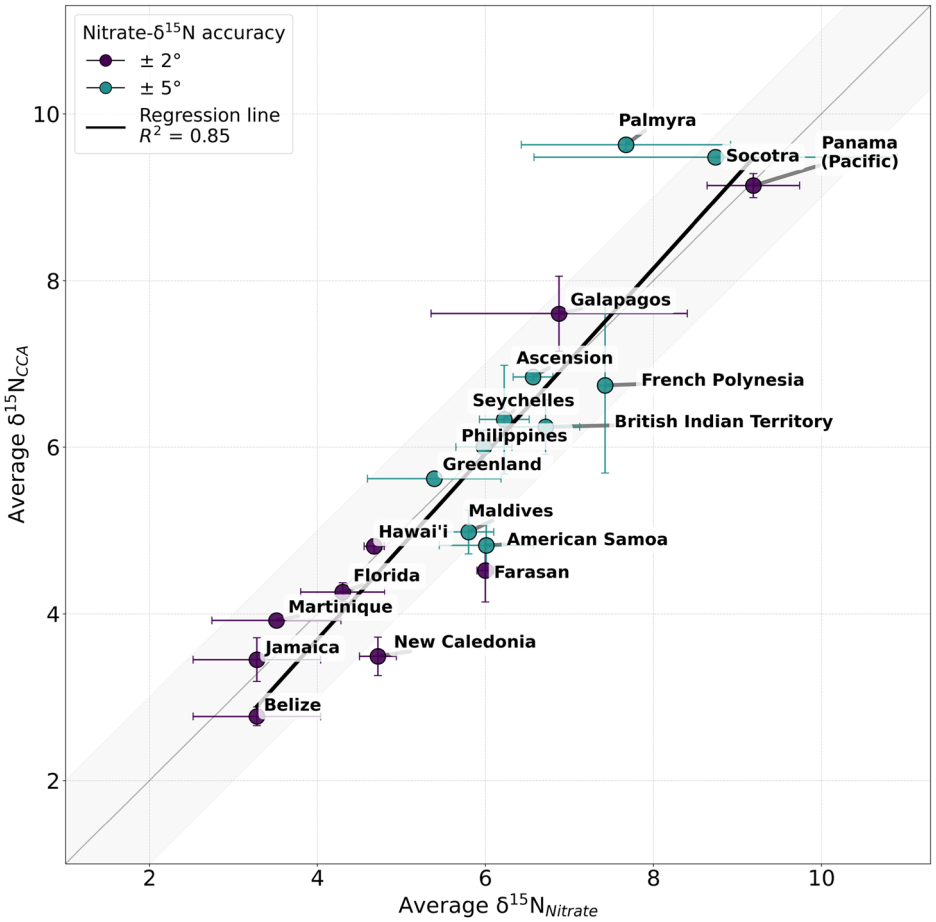

Fig. 3 | Global compilation of $\delta^{15}N_{CCA}$ and nitrate concentration-weighted $\delta^{15}N$ ($\delta^{15}N_{Nitrate}$). Comparison between nitrogen isotopic composition of the concentration-weighted nitrate (0–200 m water depth) and the $\delta^{15}N_{CCA}$ across 19 locations that had reliable $\delta^{15}N_{Nitrate}$ data and showed complete nitrate consumption at the surface. Data agree well ($r^2 = 0.85$) within 1‰ (indicated as the shaded region around the 1:1 line). Nitrate $\delta^{15}N$ data are colour-coded based on values within either ±2° or ±5° of latitude and longitude from each $\delta^{15}N_{CCA}$ location, with the search area determined by local data availability. Standard deviations are given for both $\delta^{15}N_{Nitrate}$ and $\delta^{15}N_{CCA}$.

ecosystem engineers and their ability to preserve primary geochemical signatures[52,53], which is complemented by a continuous, well-preserved fossil record throughout the Phanerozoic[54]. CCA have been shown to react sensitively to changes in seawater temperature and pH, raising their potential for palaeoceanographic reconstructions[47,52,53].

Our global calibration between $\delta^{15}N_{Nitrate}$ and $\delta^{15}N_{CCA}$ emphasizes the suitability of CCA as recorders of the marine N cycle akin to most symbiont-bearing foraminifera or corals (Fig. 3)[22,26,55]. The good agreement between $\delta^{15}N_{CCA}$ and $\delta^{15}N_{Nitrate}$ values (Fig. 3) is consistent with CCA assimilating dissolved N directly from ambient seawater with negligible isotopic fractionation[56]. However, the $\delta^{15}N$ of nitrate in the euphotic zone is often substantially higher than the $\delta^{15}N$ of the nitrate supply from the shallow subsurface due to nitrate assimilation by phytoplankton. Moreover, ammonium is an additional potential inorganic N source for CCA. Thus, the explanation for the tight correlation between $\delta^{15}N_{CCA}$ and $\delta^{15}N_{Nitrate}$ deserves deeper consideration.

In experimental systems, CCA exhibit a greater affinity for ammonium than for nitrate at a given concentration[49]. This is a common observation across algal taxa[57] and presumably reflects the lower energetic cost of assimilating reduced nitrogen species[58]. Ammonium is central to the regenerative N cycle of the euphotic zone, and the ammonium produced in the surface ocean by regeneration (i.e., heterotrophic metabolism and organic N decomposition) is inferred to have a lower $\delta^{15}N$ than the subsurface nitrate supply[59,60], as metabolism and bacterial organic N decomposition occur with isotopic fractionation in surface waters, preferentially breaking ^{14}N-containing chemical bonds[61]. All else equal, ammonium assimilation by CCA would tend to lower $\delta^{15}N_{CCA}$ relative to the $\delta^{15}N$ of the nitrate supply to the euphotic zone, counter to the observations.

There are a number of potential explanations for the lack of a clear isotopic signal of ammonium assimilation in our encrusting CCA. First, CCA are eukaryotic algae. In the subtropical open ocean, despite the scarcity of nitrate, eukaryotes are observed to specialize in its assimilation, in contrast to prokaryotes, which appear to be heavily reliant on ammonium[60,62,63]. Larger eukaryotes such as diatoms demonstrate a particularly strong specialization on nitrate assimiliation[64]. CCA may similarly specialize in nitrate assimilation. Furthermore, research comparing free-living and encrusting coralline algae found that free-living forms, such as *Arthrocardia* sp., have significantly higher maximum uptake rates for ammonia than encrusting species, suggesting that morphology influences nutrient uptake efficiency, possibly due to greater surface area exposure and less physical constraint compared to encrusting forms[49].

As noted above, the $\delta^{15}N$ of the nitrate supply is typically raised in the euphotic zone by phytoplanktonic nitrate assimilation. Thus, some amount of low-$\delta^{15}N$ ammonium assimilation by CCA may be offset by their assimilation of high-$\delta^{15}N$ nitrate, explaining the observation that the $\delta^{15}N$ of CCA is similar to that of the nitrate supply from the shallow subsurface. We do note a tendency for observations of $\delta^{15}N_{CCA}$ to be slightly lower (≤1‰) than subsurface nitrate $\delta^{15}N$ in the most oligotrophic environments (Supplementary Fig. 3). This may be a consequence of more CCA ammonium uptake in these environments, where regenerated N sources as well as recently fixed N can be proportionally more significant to algal growth[65].

In any case, the small offsets observed across our global dataset suggest that $\delta^{15}N_{CCA}$ is a reliable $\delta^{15}N$ proxy of the dissolved inorganic nitrogen supply to the euphotic zone (Fig. 3). CCA accrete slowly, typically 0.1–1 mm yr^{-1}[66], such that the $\delta^{15}N$ of the organic matter bound and preserved within their carbonate matrix reflects multi-year to decadal averages of ambient dissolved inorganic nitrogen, as integrated by their growth and calcification. Consequently, CCA fossil-bound $\delta^{15}N$ captures long-term trends in N source and cycling rather than instantaneous ecological responses, making them particularly suited for integratively recording

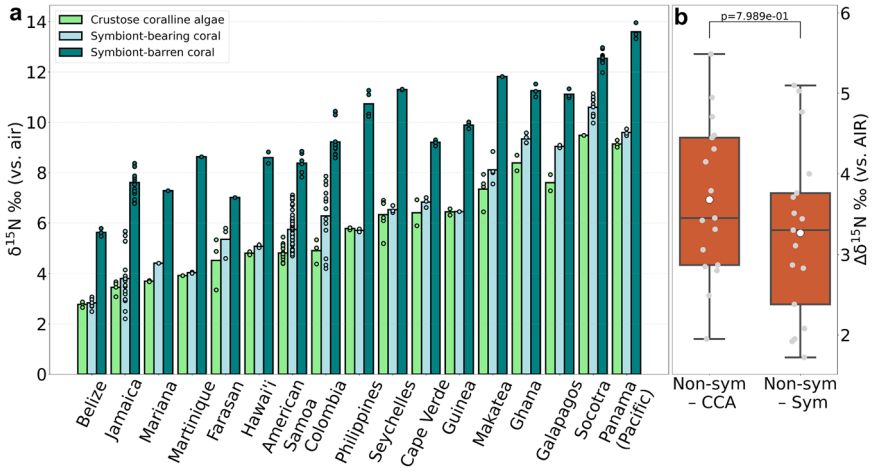

Fig. 4 | Nitrogen isotope values of crustose coralline algae (CCA), symbiont-bearing, and symbiont-barren corals. a $\delta^{15}N$ of CCA, symbiont-bearing, and symbiont-barren species from Belize, Jamaica, Mariana Islands, Martinique, Farasan (Red Sea), Hawai'i, American Samoa, the Caribbean coast of Colombia, the central Philippines, Seychelles, Cape Verde, Guinea, Makatea (French Polynesia), Ghana, Galapagos, Socotra, and the Pacific coast of Panama. **b** Average difference between symbiont-barren coral and CCA ($\Delta\delta^{15}N_{non\text{-}sym\ -\ CCA}$ = 3.68‰ ±0.97) and average difference between symbiont-barren and symbiont-bearing coral ($\Delta\delta^{15}N_{non\text{-}sym\ -\ sym}$ = 3.26‰ ±1.07) taken from all triplet locations. Comparing the ranges of $\Delta\delta^{15}N_{non\text{-}sym\ -\ CCA}$ to $\Delta\delta^{15}N_{non\text{-}sym\ -\ sym}$ yields no significant difference (t = 0.065, p = 0.79).

regional N biogeochemistry and its long-term evolution. The time-integrated $\delta^{15}N$ of CCA provides a robust baseline against which the $\delta^{15}N$ of faster-growing, mixotrophic corals can be evaluated.

BB-$\delta^{15}N$ and the feeding-excretion balance

Given that CCA sit at the base of the food web and incorporate N without the complicating influence of trophic ^{15}N enrichment, specimens approximate the $\delta^{15}N$ "baseline", that is, the average $\delta^{15}N$ of the organic matter sources to higher trophic levels, including corals. By comparison, the coral holobiont operates as a mixotroph, drawing on both particulate and dissolved nitrogen sources[34,67,68] and potentially having periods of net catabolic metabolism, during which they would efflux low-$\delta^{15}N$ metabolic ammonium. Nevertheless, in most warm-water scleractinian corals, the internal recycling of low-$\delta^{15}N$ ammonium by endosymbiotic dinoflagellates results in minimal trophic elevation of host $\delta^{15}N$[19,31], enabling symbiotic corals to reflect the $\delta^{15}N$ of the dissolved inorganic N supply to the reef environment[69], whether they acquire this N through direct assimilation or through feeding on plankton and other particulate N[65,68,70,71].

While corals have been used to track the marine N cycle, ranging from natural cyclicity[19,23,55,72] to anthropogenic disturbances[27,73,74], the striking similarity of $\delta^{15}N_{CCA}$ to the $\delta^{15}N_{sym\text{-}coral}$ across a large isotopic range in subsurface nitrate $\delta^{15}N$ (Fig. 4) suggests that CCA not only offer an independent autotrophic benchmark against which to assess coral trophic flexibility but can also be used to track the marine N cycle in places where corals do not occur (Fig. 4, Supplementary Fig. 4).

With regard to coral data, linking BB-$\delta^{15}N$ to an assimilation-excretion balance (see Methods) elevates our interpretation from a descriptive label of "mixotrophy" to a mechanistic, comparable metric of N-use efficiency across taxa and reef organisms (Fig. 1). In photosynthetic tissues, $\delta^{15}N$ is modulated by the coupling of energy-production with biosynthesis – chloroplast-driven anabolism (NADPH/ATP-powered amino-acid synthesis) and mitochondrial catabolism (de-amination and N loss) – with metabolite shuttles (e.g., malate/citrate) tuning this balance to environmental demand. By analogy, in the coral holobiont, the photosymbionts supply the anabolic arm while host and symbiont mitochondria supply the catabolic arm; kinetic isotope effects during N loss enrich retained pools in ^{15}N, whereas tight recycling suppresses this enrichment. Low reliance on symbionts (RSI) – heavy reliance of the coral on its diet for photosynthetic energy – necessarily leads to most of its assimilated N ultimately being effluxed to the environment as low-$\delta^{15}N$ metabolic ammonium, elevating coral BB-$\delta^{15}N$ (Fig. 1a). In contrast, high RSI – heavy reliance of the host on energy from its photosynthetic endosymbionts – is necessary for efficient host-symbiont N recycling, in which very little of the coral system's assimilated N (from feeding or DIN uptake) leads to the leakage of metabolic ammonium to the environment, with assimilated N instead being invested in coral or symbiont anabolism, in which case the $\delta^{15}N$ of the host-symbiont system is similar to that of its assimilated N (Fig. 1b). From this perspective, coral system autotrophy (high RSI) or heterotrophy (low RSI) is separate from the question of feeding vs. DIN acquisition for N uptake: Even when feeding is the sole N source to the coral host-symbiont system, the coral host may be nearly entirely dependent on the symbionts for photosynthetic energy, i.e., have a high RSI. This will be reflected by a lack of metabolic ammonium efflux relative to other N fates, such as coral growth.

Corals' N acquisition includes food from a range of trophic levels, such as zooplankton and detrital organic matter[37,67,75]. As such, symbiotic coral $\delta^{15}N$ values range between baseline values and one trophic enrichment factor[65]. The amplitude of the $\delta^{15}N$ offset can be interpreted as a signature of incomplete reliance on photosymbionts (low RSI; to the right in Fig. 5) and potentially enables quantification of photosymbiont reliance plasticity across genera, independent of regional baseline $\delta^{15}N$ values (Fig. 6, Supplementary Fig. 1).

First, we evaluate the reliance on photosymbionts across the large number of species present in our collection from Jamaica and American Samoa. Reliance on photosymbiont estimates derived from paired $\delta^{15}N$ values of CCA, symbiont-bearing, and non-symbiotic corals reveals substantial variation across coral species (Fig. 5). These values, standardized against site-specific $\delta^{15}N$ baselines derived from CCA, capture the spectrum of photosymbiont reliance in coral species. Species such as *Siderastrea siderea*, *Porites furcata*, *Diploria labyrinthiformis*, *Orbicella annularis*, *Acropora* spp., and *Pocillopora damicornis* exhibited the highest RSI, suggesting a reliance on symbiont photosynthate energy and thus a lack of metabolic N leakage, consistent with their known reliance on photosynthate[33,75,76]. In contrast, species such as *Galaxea fascicularis*, *Favia pallida*, *Hydnophora* sp., *Meandrina meandrites*, and *Cladocora arbuscula* showed lower reliance on photosymbionts' energy in both Jamaica and American Samoa (Fig. 5).

However, environmental factors such as light, water movement, and nutrient availability can drive morphological and trophic adjustments, acting as confounding variables that complicate the interpretation of species-level traits and nutritional strategies[77–80]. Environmental conditions during the mid-20th century, when the Jamaican (in 1973) and American Samoan samples were collected (in 1966), were shaped primarily by natural oceanographic and geomorphological differences rather than by contemporary levels of anthropogenic nutrient enrichment. Jamaican reefs occurred within a semi-enclosed carbonate shelf system characterized by low hydrodynamic energy, restricted water exchange, and episodic turbidity driven by sediment resuspension. In contrast, American Samoan reefs were situated in high-energy, open-ocean settings with steep bathymetry and persistent wave exposure, resulting in enhanced water motion, high light penetration, and efficient flushing of local nutrient pools. These contrasting physical and biogeochemical settings impose fundamentally different metabolic constraints and resource acquisition strategies, potentially shaping the balance between autotrophy and heterotrophy across coral taxa.

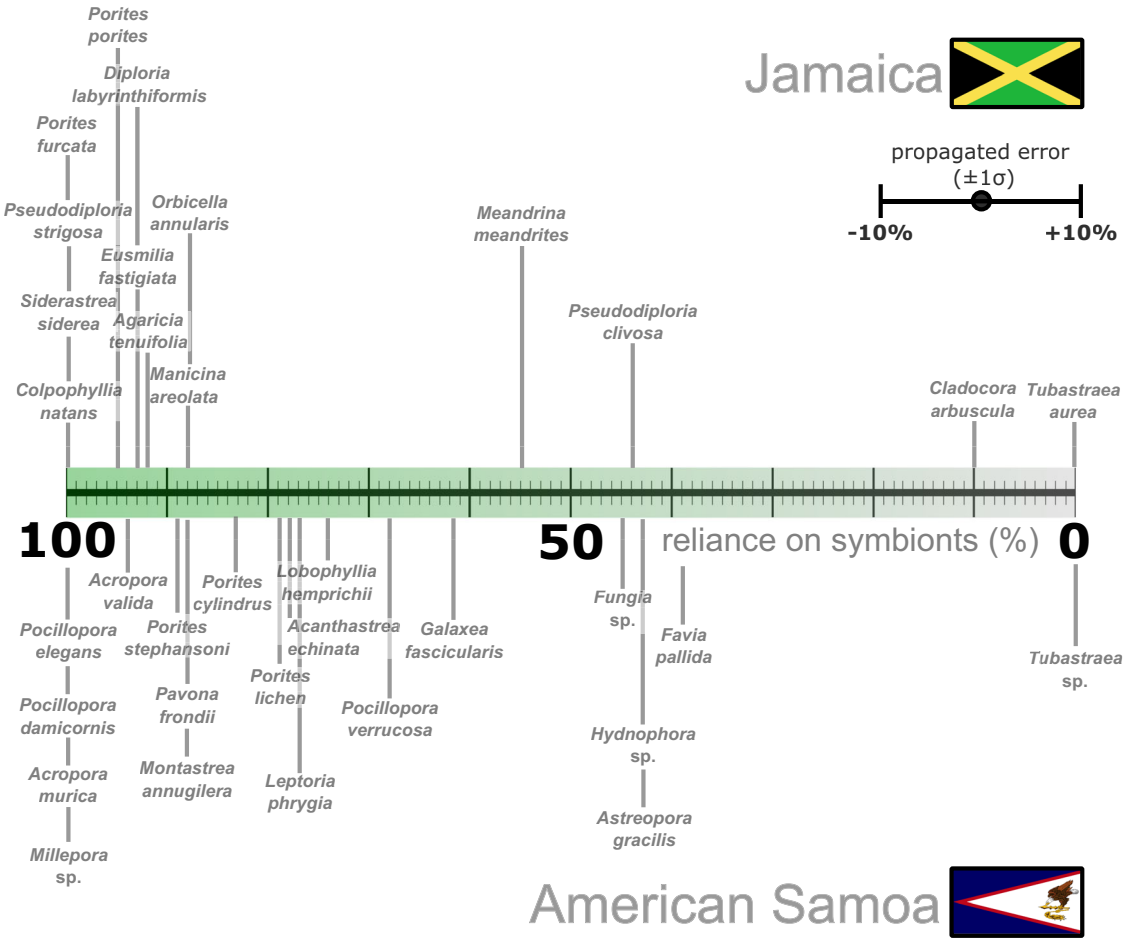

Fig. 5 | Percent energetic reliance on photosymbiosis for 33 different coral species from two distinct reefs. Across coral species, comparing two distinct reef ecosystems, the proportion of the coral host's chemical energy supply deriving directly from feeding *vs*. from symbiont photosynthesis increases to the right. The reliance on photosymbionts index = $1 - [(\delta^{15}N_{sample} - \delta^{15}N_{CCA}) / (\delta^{15}N_{nonsym\text{-}coral} - \delta^{15}N_{CCA})] \times 100$ in percentage, highlighting interspecies differences in trophic strategies within the studied reefs. Note the average propagated error of ±10% of the RSI scale.

As a result, assessing trophic plasticity at the genus level may offer a more integrative and ecologically consistent perspective.

Using the locations from our global compilation where the triplets of CCA, symbiont-bearing and -barren corals are present, we evaluate photosymbiont reliance plasticity within coral genera by examining the range in RSI across sampled individuals that yielded sufficient data from at least two different reef sites (Fig. 6 and Supplementary Fig. 3).

Pronounced differences in photosymbiont reliance plasticity are evident among coral taxa across globally distributed reef sites. *Siderastrea* spp. and *Pocillopora* spp. maintain consistently high reliance on symbiont-derived energy (>80%), indicating limited capacity to transition to feeding as its direct energy source. *Porites* spp. – particularly branching morphotypes – exhibit a wide range (~40–100%), consistent with strong heterotrophic flexibility in order to thrive under a range of environmental conditions. *Acropora* spp. occupies an intermediate position, with moderate variability and generally high photosymbiont reliance, aligning with its known vulnerability to bleaching. *Eusmilia* spp. and *Favia* spp. display lower mean reliance, reflecting greater baseline heterotrophy.

Species or genera with constrained trophic modes may exhibit optimized symbiotic nutrient recycling under stable, oligotrophic conditions but suffer disproportionately under environmental stress[44]. In contrast, genera capable of modulating their input-output dynamics may possess broader ecological niches and greater resilience under shifting conditions, including thermal anomalies, eutrophication, or turbidity events[37,76,81]. This functional trophic flexibility has implications for community composition under future climate regimes, where shifts toward more plastic coral assemblages may emerge as a response to declining photosymbiont performance.

In fact, patterns of coral persistence in Jamaica and American Samoa over the past several decades mirror the trophic strategies inferred from mid-20th-century specimens. In Jamaica, historically abundant, highly photosymbiont-dependent taxa such as branching *Acropora* have undergone dramatic declines since the 1970s due to repeated disturbances, including nutrient stress, disease outbreaks, and thermal stress, resulting in a shift from structurally complex, branching frameworks toward communities dominated by more stress-tolerant and trophically flexible taxa such as branching *Porites*. In contrast, American Samoan reefs have retained more structurally complex coral assemblages and higher cover of branching corals, consistent with the resilience advantages conferred by high-energy, high-light, well-flushed oceanic environments that support strong photosymbiosis.

When plotted alongside independent isotopic estimates (e.g., the HERS dataset)[41], our calculated values are similar across genera, reinforcing the validity of the BB-δ^{15}N-based index (Fig. 6). However, HERS estimates are a snapshot of photosymbiont reliance for one reef, similar to our snapshots from Jamaica or American Samoa (Fig. 5). When other isotope data are compiled for multiple reefs studies, they indicate that heterotrophic feeding can provide up to 33% of the amino acids required for growth in *Pocillopora damicornis*[82] and that when *Pocillopora meandrina* was compared among multiple reefs around Palmyra, on average 41% of essential amino acids were sourced directly from heterotrophic feeding (i.e., without resynthesis by the photosymbionts), with broad ranges (±50%) between the reef sites

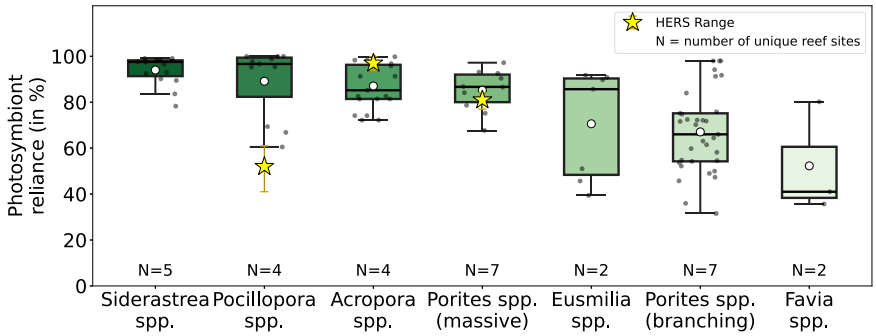

Fig. 6 | Photosymbiont reliance plasticity of seven coral genera. Data illustrating the variability in photosymbiont reliance across different coral genera, which reflects the plasticity in resource use and, thus, in trophic strategies. The data may reflect how various coral genera adapt their nutritional strategy in response to environmental conditions and available resources, highlighting intergeneric differences in resource-use flexibility. The Host Evaluation: Reliance on Symbionts (HERS) dataset[41] is plotted alongside our data.

studied[83], which suggests that trophic plasticity is an inherent nutritional strategy of almost all corals.

The differential persistence of coral taxa across distinct oceanographic regions highlights that species with constrained trophic strategies are more vulnerable when environmental conditions degrade, whereas taxa with greater heterotrophic capacity retain functional advantages under disturbance. This pattern mirrors broader ecological predictions that rapid climate warming disproportionately favours generalist and opportunistic taxa across both terrestrial and marine systems, at the expense of specialists with narrow resource or physiological niches[84]. This correspondence between historical ecological trajectories and trophic strategy suggests that the RSI framework could be used to contextualize community restructuring and species-specific resilience under contrasting environmental regimes on contemporary reefs.

Implications for the historical/geological record

Despite growing recognition of the importance of heterotrophy for coral survival under stress, its role in the response of coral reef systems to ongoing anthropogenic stressors remains poorly constrained. Biomineral-bound $\delta^{15}N$ data of coral skeletons offer a unique opportunity to infer the presence and absence of photosymbiosis over geological timescales[24,31,32,85]. When analysed in concert with $\delta^{15}N_{CCA}$ – used here as an autotrophic baseline – and purely heterotrophic corals, differences in $\delta^{15}N$ among coeval coral taxa can serve as a proxy for trophic positioning across the historical record. This isotopic spacing provides a window into mixotrophic strategies across time and taxa, enabling novel inferences about the adaptive significance of heterotrophy in reef ecosystems.

While assessing absolute heterotrophy in fossil reefs may be complicated by increasing age uncertainties in ancient reefal deposits, this triplet approach can inform whether certain coral species have shifted their nutritional pathways over time. Such comparisons are particularly valuable in the context of major environmental perturbations or reef turnovers, where differential trophic strategies may have shaped survival outcomes[86]. As BB-$\delta^{15}N$ datasets expand, this proxy has the potential to illuminate how shifts in nutrient availability, symbiotic dependencies, and feeding strategies have influenced coral resilience and reef composition throughout Earth history.

At the same time, the comparative approach between corals and CCA not only elucidates the trophic dynamics of past marine environments but also sheds light on the evolution of photosymbiotic relationships in general, offering insights into how these ecosystems responded to climatic and environmental shifts. Moreover, the use of CCA in palaeoceanographic studies could enhance our understanding of the long-term ecological processes that have shaped the marine biosphere during geological periods from which corals are not preserved.

Methods

Materials

CCA and coral skeletons were obtained from several collections to encompass a broad range of oceanographic and biogeochemical regimes across the tropical and subtropical oceans (Table 1). A total of 30 sites were included, spanning the Atlantic, Pacific, and Indian Ocean basins. Samples were sourced from curated reference collections at the Senckenberg Research Institute and Natural History Museum (Frankfurt am Main, Germany) and the Smithsonian National Museum of Natural History (Washington, DC, USA), the University of Toronto, or from the Max-Planck Institute for Chemistry, supplemented by archived specimens from institutional repositories and legacy expeditions.

The dataset includes two major sample types: (i) coral-CCA pairs ($n = 17$), comprising co-occurring coral and encrusting CCA fragments from the same reef or collection lot, and (ii) CCA-only samples ($n = 13$) from sites where paired coral material was unavailable. Coral–CCA pairs were preferentially selected from shallow fore-reef or back-reef habitats (<15 m) to minimize depth-related isotopic offsets and to represent comparable environmental exposure. Geographic coverage includes representative sites from the Caribbean (Belize, Jamaica, Martinique, Colombia, Panama), central and western Pacific (Mariana, Palmyra, Hawai'i, American Samoa, French Polynesia, Japan, Indonesia), Indian Ocean (Seychelles, Maldives, La Réunion, British Indian Territory, Oman), and Red Sea (Farasan) and the open Atlantic Ocean (Cape Verde, Ghana, Socotra, Guinea, and Ascension).

To estimate reliance on symbionts from symbiont-bearing corals, three calcifying reef taxa were targeted that collectively span the autotrophy-heterotrophy continuum: CCA, symbiont-bearing scleractinian corals, and the symbiont-barren coral *Tubastraea* spp. Encrusting CCA were selected because they are obligate photoautotrophs that mainly assimilate DIN from ambient seawater without the isotopic modification that can occur with catabolic N excretion, thus representing a pure autotrophic baseline for $\delta^{15}N$. In contrast, *Tubastraea* spp., which is non-symbiotic, feeds on planktonic N pools, metabolizes them, and excretes DIN with an isotopic fractionation associated with metabolism, raising the coral's $\delta^{15}N$ relative to its planktonic sources[20]. Symbiont-bearing corals, due to their tendency to recycle metabolic N, only partially express this "trophic" $\delta^{15}N$ elevation, with less expression and thus a lower $\delta^{15}N$ when metabolic N is more completely retained for endosymbiont photosynthetic growth[19,24,31]. Comparing biomineral-bound $\delta^{15}N$ (BB-$\delta^{15}N$) among these groups allows for quantitative assessment of trophic dependence and nutrient source partitioning across reef environments, providing a mechanistic framework for interpreting isotopic offsets as indicators of autotrophic-to-heterotrophic plasticity in the face of baseline $\delta^{15}N$ variability.

Biomineral-bound $\delta^{15}N$ data

Sample material was carefully extracted from CCA fragments using a millimetre drill bit attached to a hand-held Dremel tool. Bulk samples were taken from free-living CCA (rhodoliths) by milling into the specimen at several spots. For encrusting CCA, material was sampled by drilling across the surface to ensure samples were purely CCA. For the CCA-coral triplet comparison, only those samples were used where CCA was in direct contact with either the symbiotic or non-symbiotic coral and where all three specimens were collected from the same location and time.

Table 1 | Overview of sampling locations, geographic coordinates, collection context, and specimen types included in this study

Location	Lat	Long	Category	Coral Species	CCA Type	Date of collection	Source
American Samoa	−14.263	−170.614	Coral-CCA pair	multiple	encrusting	1966	Senckenberg Research Institute and Natural History Museum Frankfurt
Belize	16.800	-88.083	Coral-CCA pair	Orbicella annularis	encrusting	2024	Senckenberg Research Institute and Natural History Museum Frankfurt
Jamaica	18.250	−77.650	Coral-CCA pair	multiple	encrusting	1973	Senckenberg Research Institute and Natural History Museum Frankfurt
Martinique	14.633	−61.017	Coral-CCA pair	Orbicella annularis	encrusting	1999	Senckenberg Research Institute and Natural History Museum Frankfurt
Mariana	16.700	145.800	Coral-CCA pair	Porites sp.	encrusting	N/A	Senckenberg Research Institute and Natural History Museum Frankfurt
Farasan	16.700	42.450	Coral-CCA pair	Porites sp.	encrusting	N/A	Senckenberg Research Institute and Natural History Museum Frankfurt
Cape Verde	15.117	−23.600	Coral-CCA pair	multiple	encrusting	N/A	Senckenberg Research Institute and Natural History Museum Frankfurt
Guinea	9.617	−13.920	Coral-CCA pair	multiple	encrusting	N/A	Senckenberg Research Institute and Natural History Museum Frankfurt
Makatea	−15.820	−148.250	Coral-CCA pair	Porites sp.	encrusting	N/A	Smithsonian National Museum of Natural History
Colombia	11.233	−74.200	Coral-CCA pair	multiple	encrusting	1978	Senckenberg Research Institute and Natural History Museum Frankfurt
Galapagos	0.308	−90.430	Coral-CCA pair	Porites sp.	encrusting	2020	Max-Planck Institute for Chemistry
Ghana	5.100	−0.250	Coral-CCA pair	multiple	encrusting	N/A	Senckenberg Research Institute and Natural History Museum Frankfurt
Socotra	12.483	53.867	Coral-CCA pair	multiple	encrusting	2003	Senckenberg Research Institute and Natural History Museum Frankfurt
Philippines	9.495	123.225	Coral-CCA pair	Porites sp.	encrusting	N/A	Smithsonian National Museum of Natural History
Hawai'i	21.470	−157.720	Coral-CCA pair	Porites sp.	encrusting	N/A	Smithsonian National Museum of Natural History
Seychelles	−4.630	55.510	Coral-CCA pair	Porites sp.	encrusting	N/A	Max-Planck Institute for Chemistry
Panama	7.619	−81.710	Coral-CCA pair	Porites sp.	encrusting	2022	Max-Planck Institute for Chemistry
Easter Island	−27.110	−109.350	CCA only	N/A	encrusting	N/A	University of Toronto
Palmyra	5.880	−162.080	CCA only	N/A	encrusting	N/A	University of Toronto
Greenland	64.180	−51.720	CCA only	N/A	encrusting	N/A	University of Toronto
La Reunion	−21.110	55.530	CCA only	N/A	encrusting	N/A	Max-Planck Institute for Chemistry
New Caledonia	−21.500	165.500	CCA only	N/A	encrusting	2021	Max-Planck Institute for Chemistry
Ascension	−7.950	−14.380	CCA only	N/A	encrusting	N/A	Smithsonian National Museum of Natural History
Oman	22.520	59.790	CCA only	N/A	encrusting	N/A	Smithsonian National Museum of Natural History
Maldives	3.200	73.220	CCA only	N/A	encrusting	N/A	Smithsonian National Museum of Natural History
French Polynesia	−17.540	−149.570	CCA only	N/A	encrusting	N/A	Smithsonian National Museum of Natural History
Japan	26.630	127.850	CCA only	N/A	encrusting	N/A	Smithsonian National Museum of Natural History
Indonesia	−10.020	115.090	CCA only	N/A	encrusting	N/A	Smithsonian National Museum of Natural History
British Indian Territory	−6.010	71.510	CCA only	N/A	encrusting	N/A	Smithsonian National Museum of Natural History
Florida	24.628	−82.870	CCA only	N/A	encrusting	N/A	Smithsonian National Museum of Natural History

The dataset comprises 30 globally distributed reef sites spanning the Caribbean, Pacific, Indian Ocean, and Red Sea. Sites are categorized as Coral-CCA pairs, where both crustose coralline algae (CCA). All CCA samples derive from encrusting morphotypes, ensuring ecological and spatial fidelity to the local reef environment and enabling direct comparison with co-occurring corals when present. Collection years range from 1966 to 2024, with specimens sourced from major natural history repositories including the Senckenberg Research Institute and Natural History Museum Frankfurt, Smithsonian National Museum of Natural History, Max-Planck Institute for Chemistry, and the University of Toronto.

The BB-$\delta^{15}N$ measurements were also performed at the Max-Planck Institute for Chemistry (MPIC) using the persulfate oxidation-denitrifier method[87,88], first applied to corals by Wang et al.[19,20], with modifications described by Moretti et al.[89]. Coarse powder (8 ± 0.5 mg) was weighed into a pre-combusted 4 ml VWR borosilicate glass vial, which was filled with 4.25 ml sodium hypochlorite and left on a shaker at 120 revolutions per min for at least 24 h. The sodium hypochlorite was removed the next day with a pre-combusted glass pipette attached to a vacuum line set at 500 mbar. Samples were then rinsed three times with Milli-Q water (4 ml; 18.2 MΩ cm^{-1} at 25 °C) and left to dry at 60 °C overnight.

Cleaned sample material was then weighed into a new 4 ml VWR borosilicate glass vial, and the powder was dissolved with 4 N hydrochloric acid to release skeletal organic matter, which was thereafter oxidized to nitrate using 3 ml of a potassium peroxydisulfate oxidative reactant solution for each sample. The method utilizes a strain of the denitrifying bacteria *Pseudomonas chlororaphis* that lacks an active nitrous oxide reductase and converts nitrate to N_2O quantitatively[88]. 1 ml volume of concentrated *Pseudomonas chlororaphis* was injected into the growth medium (800 ml) and left for 4–6 days to grow in the dark at room temperature on a shaking rack. Once the bacteria had grown sufficiently, the medium was transferred to autoclaved polyethylene bottles and centrifuged at ~8,800 × g for 10 min. The supernatant was then discarded, and the remaining bacterial pellet was resuspended in a buffered (pH 6.3) resuspension medium. From this, 3 ml aliquots were pipetted into separate muffled glass vials (20 ml), each of which was capped with a septum and tightly sealed before being placed upside-down on a needle rack with a small additional needle for venting. The needle rack supplies a continuous flow of N_2 for at least 3 hours to replace the internal atmosphere and dissolved gases with pure N_2. The bacteria vials were removed from the rack, and the oxidized sample (~0.5 ml) was injected into each bacteria vial. Once injected, the bacteria vials were kept in the dark for 2–3 h to ensure the quantitative transformation of nitrate to nitrous oxide before being frozen at −21 °C.

The $\delta^{15}N$ of the N_2O was then determined by a purpose-built automated system for extraction and purification coupled to a Thermo MAT253 Plus stable isotope ratio mass spectrometer[90,91]. Long-term precision was determined by analysing internal carbonate standards with each sample batch, which yielded an average reproducibility of ±0.2‰ (1 SD).

Degree of heterotrophy assessment

Two reef collections, from Jamaica and American Samoa, yielded a good test case to assess mixotrophy across a range of coral species given that coral and CCA specimens were collected from the same reef at the same time (Fig. 5). This ensured that the surface layer of the coral skeleton could be sampled to minimize the BB-$\delta^{15}N$ variability that can occur due to temporal $\delta^{15}N$ changes when sampling deeper into the specimens (i.e., different years of skeletal material).

We operationalize this by anchoring each reef to CCA (autotrophic end-member) and *Tubastraea* spp. (heterotrophic end-member) and expressing each coral's position along the autotrophy – heterotrophy continuum as the RSI, which serves as a practical proxy for relative photosymbiont reliance across reefs. Standardization was performed using the formula:

$$\mathrm{RSI} = 1 - \left[\frac{\left(\delta^{15}N_{\{coral\ sample\}} - \delta^{15}N_{\{CCA\}}\right)}{\left(\delta^{15}N_{\{\mathrm{non-sym\ coral}\}} - \delta^{15}N_{\{CCA\}}\right)}\right] \times 100 \quad (1)$$

where the index is calculated based on the $\delta^{15}N_{sample}$ minus the $\delta^{15}N$ of the autotrophic end-member ($\delta^{15}N_{CCA}$) and is then standardized to the $\Delta\delta^{15}N$ (the difference between the heterotrophic end-member $\delta^{15}N$ of *Tubastraea* spp., and the autotrophic end-member $\delta^{15}N$ of CCA for any given reef). This equation allows for the interpretation of any given coral BB-$\delta^{15}N$ value on a scale of 100 = autotrophic/recycling-dominated and 0 = heterotrophic/catabolic-dominated. To evaluate the influence of analytical uncertainty in $\delta^{15}N$ measurements on the derived RSI, we performed a simple error-propagation analysis.

The combined propagated error for RSI was calculated for average uncertainties of the three groups used in the calculation:

σ_A = ± 0.21‰ of average A, where A = $\delta^{15}N_{CCA}$ for each location,

σ_B = ± 0.31‰ of average B, where B = $\delta^{15}N_{coral\ sample}$ for each location,

σ_C = ± 0.23‰ of average C, where C = $\delta^{15}N_{Tubastrea}$ for each location,

yielding a mean propagated uncertainty:

$$\sigma_z = 100\sqrt{\left(\frac{B-C}{(C-A)^2}\cdot\sigma_A\right)^2 + \left(\frac{\sigma_B}{C-A}\right)^2 + \left(\frac{B-A}{(C-A)^2}\cdot\sigma_C\right)^2} \quad (2)$$

yields an average σ_Z of ±10% on the RSI scale (Fig. 5).

Ranges of heterotrophy (heterotrophic plasticity) were calculated on a subset of coral genera or species that were found at multiple sampling locations (Supplementary Fig. 2). This enabled comparisons of potential genera- or species-specific adaptive strategies across environmental and geographic ranges (Fig. 6).

Nitrate $\delta^{15}N$ data

Nitrate $\delta^{15}N$ data were mainly sourced from the database compiled by Fripiat et al. 2021[7] and individual publications, for example, from the Indian Ocean, the Red Sea, or New Caledonia[92,93]. Some new data (unpublished from the Caribbean and Eastern Tropical Pacific) were generated from samples obtained with the research vessel R/V Eugen Seibold[94].

To characterize the isotopic composition of subsurface nitrate, we calculated concentration-weighted average $\delta^{15}N$ values ($\delta^{15}N_{Nitrate}$) across depth profiles. Only data between 0 to 200 m were included to capture the nutricline while minimizing surface variability. For each profile, the concentration-weighted $\delta^{15}N$ was computed using the formula:

$$\delta^{15}N_{weighted} = \sum_i(\delta^{15}N_i \times [NO_3^-]_i)/\sum_i[NO_3^-]_i$$

where $\delta^{15}N_i$ and $[NO_3^-]_i$ represent the $\delta^{15}N$ and nitrate concentration at each sampled depth interval i, respectively. The associated standard deviation was calculated using the weighted variance to reflect vertical heterogeneity in both concentration and isotopic composition. These values were used as nitrate $\delta^{15}N$ baselines for comparison with $\delta^{15}N_{CCA}$, where sufficient data were available within a range of ±2° and ±5° in latitude and longitude around the $\delta^{15}N_{CCA}$ sample location (Figs. 2 and 3, Supplementary Fig. 1).

Analysis of seawater

$\delta^{15}N$ of $NO_3^- + NO_2^-$ and NO_3^--only were measured using the denitrifier method[88] at the Martínez-García Laboratory, MPIC, following the protocols of[91]. About 5 nmol of $NO_3^- + NO_2^-$ or NO_3^- was quantitatively converted to N_2O gas by a strain of the denitrifying bacteria *Pseudomonas aureofaciens* that lacks an active N_2O reductase. The $\delta^{15}N$ of the N_2O was determined as above.

Statistics

All data were imported to a Python3 Jupyter Notebook (Version 5.7.4) using the Pandas library. Data were plotted with Seaborn/Matplotlib. Statistical tests were done using scipy.stats library. Associated standard deviations of concentration-weighted $\delta^{15}N_{Nitrate}$ were calculated using the weighted variance to reflect vertical heterogeneity in both concentration and isotopic composition. Standard deviations of BB-$\delta^{15}N$ are given as ±1 SD.

Reporting summary

Further information on research design is available in the Nature Portfolio Reporting Summary linked to this article.

Data availability

All data are publicly available on Zenodo (https://doi.org/10.5281/zenodo.19017991).

Code availability

Codes used for the figures and data analyses are available on GitHub (https://github.com/marinejon/Crustose-Coralline-Algae-as-a-Proxy-for-Marine-Nitrogen-Cycling-and-Coral-Trophic-Strategies).

Received: 26 August 2025; Accepted: 19 March 2026;
Published online: 10 April 2026

References

1. Sarmiento, J. L. & Gruber, N. *Ocean Biogeochemical Dynamics*. (Princeton University Press, 2006). https://doi.org/10.2307/j.ctt3fgxqx.
2. Deutsch, C., Sarmiento, J. L., Sigman, D. M., Gruber, N. & Dunne, J. P. Spatial coupling of nitrogen inputs and losses in the ocean. *Nature* **445**, 163–167 (2007).
3. Falkowski, P. G. Evolution of the nitrogen cycle and its influence on the biological sequestration of CO2 in the ocean. *Nature* **387**, 272–275 (1997).
4. Altabet, M. A. & Francois, R. The Use of Nitrogen Isotopic Ratio for Reconstruction of Past Changes in Surface Ocean Nutrient Utilization. in *Carbon Cycling in the Glacial Ocean: Constraints on the Ocean's Role in Global Change* (eds Zahn, R., Pedersen, T. F., Kaminski, M. A. & Labeyrie, L.) 281–306 (Springer Berlin Heidelberg, Berlin, Heidelberg, 1994). https://doi.org/10.1007/978-3-642-78737-9_12.
5. Ren, H. et al. Foraminiferal isotope evidence of reduced nitrogen fixation in the ice age Atlantic Ocean. *Science* **323**, 244–248 (2009).
6. Fripiat, F. et al. The impact of incomplete nutrient consumption in the Southern Ocean on Global Mean Ocean Nitrate δ15N. *Glob. Biogeochem. Cycles* **37**, e2022GB007442 (2023).
7. Fripiat, F. et al. Nitrogen isotopic constraints on nutrient transport to the upper ocean. *Nat. Geosci.* **14**, 855–861 (2021).
8. Brandes, J. A. & Devol, A. H. Isotopic fractionation of oxygen and nitrogen in coastal marine sediments. *Geochim. Cosmochim. Acta* **61**, 1793–1801 (1997).
9. Sweeney, R. E. & Kaplan, I. R. Natural abundances of 15N as a source indicator for near-shore marine sedimentary and dissolved nitrogen. *Mar. Chem.* **9**, 81–94 (1980).
10. Lehmann, M. F. et al. The distribution of nitrate 15N/14N in marine sediments and the impact of benthic nitrogen loss on the isotopic composition of oceanic nitrate. *Geochim. Cosmochim. Acta* **71**, 5384–5404 (2007).
11. Granger, J. et al. Coupled nitrification-denitrification in sediment of the eastern Bering Sea shelf leads to 15N enrichment of fixed N in shelf waters. *J. Geophys. Res.: Oceans* **116**, 1–18 (2011).
12. Lehmann, M. F., Sigman, D. M. & Berelson, W. M. Coupling the 15N/14N and 18O/16O of nitrate as a constraint on benthic nitrogen cycling. *Mar. Chem.* **88**, 1–20 (2004).
13. Ren, H., Sigman, D. M., Thunell, R. C. & Prokopenko, M. G. Nitrogen isotopic composition of planktonic foraminifera from the modern ocean and recent sediments. *Limnol. Oceanogr.* **57**, 1011–1024 (2012).
14. Smart, S. M. et al. The nitrogen isotopic composition of tissue and shell-bound organic matter of Planktic Foraminifera in Southern Ocean Surface Waters. *Geochem., Geophys. Geosyst.* **21**, e2019GC008440 (2020).
15. Smart, S. M. et al. Ground-truthing the planktic foraminifer-bound nitrogen isotope paleo-proxy in the Sargasso Sea. *Geochim. Cosmochim. Acta* **235**, 463–482 (2018).
16. Granger, R. et al. Tracking Agulhas Leakage in the South Atlantic Using Modern Planktic Foraminifera Nitrogen Isotopes. *Geochem., Geophys. Geosyst.* **25**, e2023GC011190 (2024).
17. Robinson, R. S., Brunelle, B. G. & Sigman, D. M. Revisiting nutrient utilization in the glacial Antarctic: Evidence from a new method for diatom-bound N isotopic analysis. *Paleoceanography* **19**, 1–13 (2004).
18. Sigman, D. M., Altabet, M. A., Francois, R., McCorkle, D. C. & Gaillard, J.-F. The isotopic composition of diatom-bound nitrogen in Southern Ocean sediments. *Paleoceanography* **14**, 118–134 (1999).
19. Wang, X. T. et al. Isotopic composition of skeleton-bound organic nitrogen in reef-building symbiotic corals: A new method and proxy evaluation at Bermuda. *Geochim. Cosmochim.Acta* **148**, 179–190 (2015).
20. Wang, X. T. et al. Isotopic composition of carbonate-bound organic nitrogen in deep-sea scleractinian corals: A new window into past biogeochemical change. *Earth Planet. Sci. Lett.* **400**, 243–250 (2014).
21. Martínez-García, A. et al. Laboratory Assessment of the Impact of Chemical Oxidation, Mineral Dissolution, and Heating on the Nitrogen Isotopic Composition of Fossil-Bound Organic Matter. *Geochem., Geophys. Geosyst.* **23**, e2022GC010396 (2022).
22. Auderset, A. et al. Enhanced ocean oxygenation during Cenozoic warm periods. *Nature* **609**, 77–82 (2022).
23. Duprey, N. N. et al. Decadal oscillations in the ocean's largest oxygen-deficient zone. *Science* **386**, 1019–1024 (2024).
24. Jung, J. et al. Coral photosymbiosis on Mid-Devonian reefs. *Nature* **636**, 647–653 (2024).
25. Kast, E. R. et al. Nitrogen isotope evidence for expanded ocean suboxia in the early Cenozoic. *Science* **364**, 386–389 (2019).
26. Moretti, S. et al. Oxygen rise in the tropical upper ocean during the Paleocene-Eocene Thermal Maximum. *Science* **383**, 727–731 (2024).
27. Ren, H. et al. 21st-century rise in anthropogenic nitrogen deposition on a remote coral reef. *Science* **356**, 749–752 (2017).
28. Auderset, A. et al. Effects of photosymbiosis and related processes on planktic foraminifera-bound nitrogen isotopes in South Atlantic sediments. *Biogeosciences* **22**, 1887–1905 (2025).
29. Deniro, M. J. & Epstein, S. Influence of diet on the distribution of nitrogen isotopes in animals. *Geochim. Cosmochim. Acta* **45**, 341–351 (1981).
30. Minagawa, M. & Wada, E. Stepwise enrichment of 15N along food chains: Further evidence and the relation between δ15N and animal age. *Geochim. Cosmochim. Acta* **48**, 1135–1140 (1984).
31. Frankowiak, K. et al. Photosymbiosis and the expansion of shallow-water corals. *Sci. Adv.* **2**, e1601122 (2016).
32. Muscatine, L. et al. Stable isotopes (δ13C and δ15N) of organic matrix from coral skeleton. *Proc. Natl. Acad. Sci.* **102**, 1525–1530 (2005).
33. Conti-Jerpe, I. E. et al. Trophic strategy and bleaching resistance in reef-building corals. *Sci. Adv.* **6**, eaaz5443 (2020).
34. Price, J. T., McLachlan, R. H., Jury, C. P., Toonen, R. J. & Grottoli, A. G. Isotopic approaches to estimating the contribution of heterotrophic sources to Hawaiian corals. *Limnol. Oceanogr.* **66**, 2393–2407 (2021).
35. Thibault, M. et al. Seabird-Derived Nutrients Supply Modulates the Trophic Strategies of Mixotrophic Corals. *Front. Mar. Sci.* **8**, 790408 (2022).
36. Straub, M. et al. Nitrogen isotopic composition as a gauge of tumor cell anabolism-to-catabolism ratio. *Sci. Rep.* **13**, 19796 (2023).
37. Houlbrèque, F. & Ferrier-Pagès, C. Heterotrophy in tropical scleractinian corals. *Biol. Rev. Camb. Philos. Soc.* **84**, 1–17 (2009).
38. Palardy, J. E., Rodrigues, L. J. & Grottoli, A. G. The importance of zooplankton to the daily metabolic carbon requirements of healthy and bleached corals at two depths. *J. Exp. Mar. Biol. Ecol.* **367**, 180–188 (2008).
39. Levy, O. et al. Complex Diel Cycles of Gene Expression in Coral-Algal Symbiosis. *Science* **331**, 175–175 (2011).

40. Chei, E., Conti-Jerpe, I. E., Pons, L. & Baker, D. M. Changes within the coral symbiosis underpin seasonal trophic plasticity in reef corals. *ISME Commun.* **5**, ycae162 (2025).
41. Guibert, I. et al. Trophic niche partitioning in giant clams. *Commun. Biol.* **9**, 48 (2024).
42. Klaus, J. S., Murray, S. T., Swart, P. K. & McNeill, D. F. Resource partitioning and paleoecology of neogene free-living corals as determined from skeletal stable isotope composition. *Bull. Mar. Sci.* **89**, 937–954 (2013).
43. Campoy, A. N. et al. The Origin and Correlated Evolution of Symbiosis and Coloniality in Scleractinian Corals. *Front. Mar. Sci.* **7**, https://doi.org/10.3389/fmars.2020.00461 (2020).
44. Stanley, G. D. Photosymbiosis and the Evolution of Modern Coral Reefs. *Science* **312**, 857–858 (2006).
45. McCoy, S. J. & Kamenos, N. A. Coralline algae (Rhodophyta) in a changing world: integrating ecological, physiological, and geochemical responses to global change. *J. Phycol.* **51**, 6–24 (2015).
46. Teichert, S. Attached and free-living crustose coralline algae and their functional traits in the geological record and today. *Facies* **70**, 8 (2024).
47. de Carvalho, R. T. et al. Global assessment of coralline algae mineralogy points to high vulnerability of Southwestern Atlantic reefs and rhodolith beds to ocean acidification. *Sci. Rep.* **12**, 9589 (2022).
48. Weiss, A. & Martindale, R. C. Crustose coralline algae increased framework and diversity on ancient coral reefs. *PLoS One* **12**, e0181637 (2017).
49. Nguyen, H. T. T., Pritchard, D. W. & Hepburn, C. D. Nitrogen and phosphorus ecophysiology of coralline algae. *J. Appl Phycol.* **32**, 2583–2597 (2020).
50. Doherty, J. M., Williams, B., Kline, E., Adey, W. & Thibodeau, B. Climate-modulated nutrient conditions along the labrador shelf: evidence from nitrogen isotopes in a six-hundred-year-old crustose Coralline Alga. *Paleoceanogr. Paleoclimatol.* **36**, e2020PA004149 (2021).
51. Nazir, A. et al. Anthropogenic nitrogen pollution inferred by stable isotope records of crustose coralline algae. *Mar. Pollut. Bull.* **198**, 115839 (2024).
52. Halfar, J., Steneck, R. S., Joachimski, M., Kronz, A. & Wanamaker, A. D. Jr. Coralline red algae as high-resolution climate recorders. *Geology* **36**, 463–466 (2008).
53. Hetzinger, S. et al. High-resolution analysis of trace elements in crustose coralline algae from the North Atlantic and North Pacific by laser ablation ICP-MS. *Palaeogeogr. Palaeoclimatol. Palaeoecol.* **302**, 81–94 (2011).
54. Aguirre, J., Perfectti, F. & Braga, J. C. Integrating phylogeny, molecular clocks, and the fossil record in the evolution of coralline algae (Corallinales and Sporolithales, Rhodophyta). *Paleobiology* **36**, 519–533 (2010).
55. Jung, J. et al. Equatorial upwelling of phosphorus drives Atlantic N2 fixation and Sargassum blooms. *Nat. Geosci*. 1–7 (2025) https://doi.org/10.1038/s41561-025-01812-2.
56. Dugdale, R. C. & Goering, J. J. Uptake of New and Regenerated Forms of Nitrogen in Primary Productivity. *Limnol. Oceanogr.* **12**, 196–206 (1967).
57. McNeil, M., Nothdurft, L., Erler, D., Hua, Q. & Webster, J. M. Variations in Mid- to Late Holocene Nitrogen Supply to Northern Great Barrier Reef Halimeda Macroalgal Bioherms. *Paleoceanogr. Paleoclimatol.* **36**, e2020PA003871 (2021).
58. Gutschick, V. P. Evolved Strategies in Nitrogen Acquisition by Plants. *Am. Nat.* **118**, 607–637 (1981).
59. Altabet, M. A. Variations in nitrogen isotopic composition between sinking and suspended particles: implications for nitrogen cycling and particle transformation in the open ocean. *Deep Sea Res. Part A. Oceanogr. Res. Pap.* **35**, 535–554 (1988).
60. Fawcett, S. E., Lomas, M. W., Casey, J. R., Ward, B. B. & Sigman, D. M. Assimilation of upwelled nitrate by small eukaryotes in the Sargasso Sea. *Nat. Geosci.* **4**, 717–722 (2011).
61. Möbius, J. Isotope fractionation during nitrogen remineralization (ammonification): Implications for nitrogen isotope biogeochemistry. *Geochim. Cosmochim. Acta* **105**, 422–432 (2013).
62. Fawcett, S. E., Lomas, M. W., Ward, B. B. & Sigman, D. M. The counterintuitive effect of summer-to-fall mixed layer deepening on eukaryotic new production in the Sargasso Sea. *Glob. Biogeochem. Cycles* **28**, 86–102 (2014).
63. Treibergs, L. A., Fawcett, S. E., Lomas, M. W. & Sigman, D. M. Nitrogen isotopic response of prokaryotic and eukaryotic phytoplankton to nitrate availability in Sargasso Sea surface waters. *Limnol. Oceanogr.* **59**, 972–985 (2014).
64. Fawcett, S. E. & Ward, B. B. Phytoplankton succession and nitrogen utilization during the development of an upwelling bloom. *Mar. Ecol. Prog. Ser.* **428**, 13–31 (2011).
65. Luu, V. H. et al. Nitrogen isotope ratios across the Bermuda coral reef: implications for coral nitrogen sources and the coral-bound nitrogen isotope proxy. *Front. Mar. Sci*. **12**, 1554418 (2025).
66. Adey, W. H. & Vassar, J. M. Colonization, succession and growth rates of tropical crustose coralline algae (Rhodophyta, Cryptonemiales). *Phycologia* **14**, 55–69 (1975).
67. Muscatine, L., Porter, J. W. & Kaplan, I. R. Resource partitioning by reef corals as determined from stable isotope composition. *Mar. Biol.* **100**, 185–193 (1989).
68. Rädecker, N., Pogoreutz, C., Voolstra, C. R., Wiedenmann, J. & Wild, C. Nitrogen cycling in corals: the key to understanding holobiont functioning? *Trends Microbiol.* **23**, 490–497 (2015).
69. Wang, X. T. et al. Influence of open ocean nitrogen supply on the skeletal δ15N of modern shallow-water scleractinian corals. *Earth Planet. Sci. Lett.* **441**, 125–132 (2016).
70. Davy, S. K., Allemand, D. & Weis, V. M. Cell biology of cnidarian-dinoflagellate symbiosis. *Microbiol Mol. Biol. Rev.* **76**, 229–261 (2012).
71. Ferrier-Pagès, C. & Leal, M. C. Stable isotopes as tracers of trophic interactions in marine mutualistic symbioses. *Ecol. Evol.* **9**, 723–740 (2019).
72. Wang, X. T. et al. Natural forcing of the North Atlantic nitrogen cycle in the Anthropocene. *Proc. Natl. Acad. Sci.* **115**, 10606–10611 (2018).
73. DeLong, K. L. et al. The Flower Garden Banks Siderastrea siderea coral as a candidate Global boundary Stratotype Section and Point for the Anthropocene series. *Anthropocene Rev.* **10**, 225–250 (2023).
74. Duprey, N. N. et al. Megacity development and the demise of coastal coral communities: Evidence from coral skeleton δ15N records in the Pearl River estuary. *Glob. Change Biol.* **26**, 1338–1353 (2020).
75. Fox, M. D. et al. Gradients in primary production predict trophic strategies of Mixotrophic Corals across Spatial Scales. *Curr. Biol.* **28**, 3355–3363.e4 (2018).
76. Grottoli, A. G., Rodrigues, L. J. & Palardy, J. E. Heterotrophic plasticity and resilience in bleached corals. *Nature* **440**, 1186–1189 (2006).
77. Sturaro, N., Hsieh, Y. E., Chen, Q., Wang, P. & Denis, V. Trophic plasticity of mixotrophic corals under contrasting environments. *Funct. Ecol.* **35**, 2841–2855 (2021).
78. Goodbody-Gringley, G. et al. Irradiance driven trophic plasticity in the coral Madracis pharensis from the Eastern Mediterranean. *Sci. Rep.* **14**, 3646 (2024).
79. Hoogenboom, M. O., Connolly, S. R. & Anthony, K. R. N. Interactions between morphological and physiological plasticity optimize energy acquisition in corals. *Ecology* **89**, 1144–1154 (2008).
80. Todd, P. A. Morphological plasticity in scleractinian corals. *Biol. Rev.* **83**, 315–337 (2008).
81. Anthony, K. R. & Fabricius, K. E. Shifting roles of heterotrophy and autotrophy in coral energetics under varying turbidity. *J. Exp. Mar. Biol. Ecol.* **252**, 221–253 (2000).

82. Anthony, K. R. N. Coral suspension feeding on fine particulate matter. *J. Exp. Mar. Biol. Ecol.* **232**, 85–106 (1999).
83. Fox, M. D., Elliott Smith, E. A., Smith, J. E. & Newsome, S. D. Trophic plasticity in a common reef-building coral: Insights from δ13C analysis of essential amino acids. *Funct. Ecol.* **33**, 2203–2214 (2019).
84. Clavel, J., Julliard, R. & Devictor, V. Worldwide decline of specialist species: toward a global functional homogenization? *Front. Ecol. Environ.* **9**, 222–228 (2011).
85. Tornabene, C., Martindale, R. C., Wang, X. T. & Schaller, M. F. Detecting Photosymbiosis in Fossil Scleractinian Corals. *Sci. Rep.* **7**, 9465 (2017).
86. Kiessling, W. Geologic and Biologic Controls on the Evolution of Reefs. *Annu. Rev. Ecol., Evol. Syst.* **40**, 173–192 (2009).
87. Knapp, A. N., Sigman, D. M. & Lipschultz, F. N isotopic composition of dissolved organic nitrogen and nitrate at the Bermuda Atlantic Time-series Study site. *Glob. Biogeochem. Cycles* **19**, 1–15 (2005).
88. Sigman, D. M. et al. A Bacterial Method for the Nitrogen Isotopic Analysis of Nitrate in Seawater and Freshwater. *Anal. Chem.* **73**, 4145–4153 (2001).
89. Moretti, S. et al. Analytical improvements and assessment of long-term performance of the oxidation–denitrifier method. *Rapid Commun. Mass Spectrom.* **38**, e9650 (2024).
90. Casciotti, K. L., Sigman, D. M., Hastings, M. G., Böhlke, J. K. & Hilkert, A. Measurement of the oxygen isotopic composition of nitrate in seawater and freshwater using the Denitrifier method. *Anal. Chem.* **74**, 4905–4912 (2002).
91. Weigand, M. A., Foriel, J., Barnett, B., Oleynik, S. & Sigman, D. M. Updates to instrumentation and protocols for isotopic analysis of nitrate by the denitrifier method. *Rapid Commun. Mass Spectrom.* **30**, 1365–1383 (2016).
92. Choisnard, N. et al. Tracing the fate of seabird-derived nitrogen in a coral reef using nitrate and coral skeleton nitrogen isotopes. *Limnol. Oceanogr.* **69**, 309–324 (2024).
93. Marshall, T. A. et al. The Agulhas Current Transports Signals of Local and Remote Indian Ocean Nitrogen Cycling. *J. Geophys. Res.: Oceans* **128**, e2022JC019413 (2023).
94. Schiebel, R. et al. Preface: Special Issue on Probing the Open Ocean With the Research Sailing Yacht Eugen Seibold for Climate Geochemistry. *J. Geophys. Res.: Atmos.* **129**, e2023JD040581 (2024).

Acknowledgements

This study was funded by the Max Planck Society (GHH and AMG) and the Max-Planck Graduate Center (JJ). Nicolas N. Duprey acknowledges the German Research Foundation—Project number 468591845 (awarded to A. Martínez-García) —SPP 2299/Project number 441832482 as well as the Paul Crutzen post-doctoral fellowship. KC, MD, AF and MB acknowledge funding from the U.S. National Science Foundation (#2315076). DMS acknowledges funding from the U.S. NSF Grant #1851430 and #2049416. We thank Florian Rubach, Barbara Hinnenberg, and Mareike Schmitt for technical support during sample preparation and analysis. We thank Claudia Vaga, Amanda Robinson, Andrea Quattrini and William Moser from the Smithsonian Institution in Washington D.C. All samples were acquired from major natural history repositories including the Senckenberg Research Institute and Natural History Museum Frankfurt, Smithsonian National Museum of Natural History, Max-Planck Institute for Chemistry, and the University of Toronto with no permits required other than destructive sampling permissions that were issued by the respective institute.

Author contributions

J.J., T.W. and A.M.G. conceived the study and managed the project, with A.M.G. and D.M.S. providing supervision. The methodology was developed by J.J., T.W., A.D.F., A.M.G, S.M., AB, J.H., D.M., and D.M.S. Funding was secured by G.H.H. and A.M.G. Resources were provided by J.J., T.W., DJ, NDD, C.P.M., A.O.D., R.S., C.F.G., M.B., M.J.D., A.F., and K.C. J.J., A.M.G., and D.M.S. validated the work. J.J., T.W., A.D.F., D.M.S., and A.M.G drafted the original manuscript, and all authors contributed to review and editing.

Funding

Open Access funding enabled and organized by Projekt DEAL.

Competing interests

The authors declare no competing interests.

Additional information

Supplementary information The online version contains supplementary material available at https://doi.org/10.1038/s43247-026-03459-2.

Correspondence and requests for materials should be addressed to Jonathan Jung or Alfredo Martínez-García.

Peer review information *Communications Earth and Environment* thanks the anonymous reviewers for their contribution to the peer review of this work. Primary Handling Editors: Christopher Cornwall and Martina Grecequet. A peer review file is available.